Extreme Reversal in Mechanical Anisotropy in Liquid-Liquid Interfaces Reinforced with Self-Assembled Protein Nanosheets

William Megone[1,2], Dexu Kong[1,2], Lihui Peng[1,2] and Julien E. Gautrot[1,2]

[1]Institute of Bioengineering and [2]School of Engineering and Materials Science, Queen Mary, University of London, Mile End Road, London, E1 4NS, UK.

E-mail: j.gautrot@qmul.ac.uk

Keywords: Protein nanosheets; Liquid-liquid interface; Interfacial mechanics; Mechanical anisotropy; Self-assembly.

Abstract

The structuring of liquid-liquid and liquid-air interfaces may play an important role in novel microfabrication platforms and biotechnologies, from the spontaneous formation of microfilaments from liquid droplets and the 3D printing of liquids, to the culture of stem cells on emulsions. Understanding the mechanical anisotropy of associated liquid interfaces is essential for the development of such systems. Models of AFM indentation at liquid interfaces, based on the Young-Laplace model, currently do not allow the quantification of interfacial mechanical properties of associated molecular films. This report presents such a model and compares its predictions to interfacial mechanical properties characterised via interfacial shear rheology. An extreme reversal of mechanical anisotropy of liquid-liquid interfaces is observed, upon self-assembly of protein nanosheets, by 5 orders of magnitude. Results indicate that, although interfacial rheology is more sensitive than AFM indentation to the mechanics of molecular films in the low range of interfacial mechanics, AFM indentation allows the quantification of mechanical properties of stiffer molecular films, and remains better adapted to the characterisation of small samples and enables the characterisation of local heterogeneity.

1. Introduction

The structuring of liquid interfaces plays an important role in many processes and technological platforms, from the modulation of surface tension at the air-liquid interface by lung surfactants [1], the stabilisation of foams by natural surfactant proteins of the Ranaspumin family, to protect frog eggs [2], and the mechanical strengthening of liquid interfaces for the protection of biofilms [3, 4], to the printing of liquid formulations [5] and the engineering of microdroplets [6]. Understanding how the self-assembly of surfactants, proteins and nanoparticles regulates the mechanical properties of corresponding liquid-air and liquid-liquid interfaces is essential to enable the application of these interfaces in a wide range of fields, including biotechnologies and microfabrication. In particular, understanding the inherent mechanical anisotropy of liquid interfaces, may have important implications in the development of novel technologies enabling cell culture on liquid substrates [7] and the microstructuring of liquids [6] and liquid crystalline materials [8].

Characterisation of the mechanics of liquid-liquid interfaces can be achieved via a range of techniques, including interfacial rheology [9], dilatational rheology [10] and AFM indentation [11]. Although AFM indentation has not yet been widely applied for such characterisation, it is attractive as it allows to gain local information on interfacial mechanics, and allows the study of interfaces with relatively low surface areas and volumes (e.g. microdroplets). To this aim, models enabling the dissociation of the contributions of interfacial interaction forces from the surface tension have allowed the quantitative description of AFM indentation profiles [11, 12]. These models are based on the augmented Young-Laplace equation, which describes force-indentation traces as a function of surface tension and disjoining pressure. However, models enabling the extraction of quantitative mechanical properties of molecular films underpinning the structuring of liquid interfaces have not been developed.

In this work, we report the extreme reversal in mechanical anisotropy of liquid-liquid interfaces, by five orders of magnitude, upon self-assembly of protein nanosheets. We make a direct comparison

between the AFM indentation profile of liquid-liquid interfaces and their interfacial rheology. To extract quantitative information on the mechanical properties of molecular films via AFM indentation, we develop a modified Young-Laplace model. We carry out systematic analysis of the parameter space in order to identify the range within which such quantitative analysis is meaningful. Finally, we apply force probe microscopy to the mapping of nanosheet heterogeneity. The understanding of the mechanical anisotropy of liquid-liquid interfaces will have important implications in the design of novel microdroplet systems for the microstructuring of liquids and the design of emulsion-based cell culture systems.

2. Methods

2.1. Materials

Pentafluorobenzoyl chloride (PFBC, 99%), benzoyl chloride (BC, 99%), lysozyme (BioUltra, >98%), bovine serum albumin (BSA, heat shock fraction, 98%), poly-l-lysine (PLL, M_w 30,000-70,000 Da) and 20 μm diameter silicon particles (unfunctionalised, dry powder) were all purchased from Sigma Aldrich. Blandol® White Mineral Oil was purchased from Sonneborn. 3M™ Novec™ 7500 Engineered Fluid was purchased from fluorochem. Bruker ORC 8 – 10 AFM tips were purchased from Bruker.

2.2. Preparation of interfaces

Compositions of phases used for the assembly of interfaces can be found in Supplementary Table S1. The oils with pro-surfactant (acyl chloride) were always mixed separately first, prior to introduction of the aqueous phase. Proteins were introduced after formation of the oil-water interface, allowing assembly of the corresponding protein nanosheets specifically at the interface. PLL and BSA nanosheets on fluorinated oils were allowed to assemble for 2 h, while lysozyme nanosheets on the mineral oil were allowed to assemble overnight. For samples characterised by AFM and

electrophoretic light scattering, excess protein was washed by sequential dilution in PBS (4 folds, repeated 6 times).

2.3. Tensiometer

Surface tension was measured using a Kruss K9 tensiometer. The surface tension at the interface of both mineral oil (Blandol White) and fluorinated oil (Novec 7500) was obtained using a 20 mm du Noüy ring. When testing the surface tension of the interface with a protein nanosheet the ring was left in the bottom phase and the protein added. The protein was then left for a minimum of 2 hr to deposit and then the surface tension measurement taken. Before measuring the surface tension of the interfaces the ring was calibrated against a deionised water – air interface. A minimum of three repeats for each interface were recorded.

2.4. Electrophoretic light scattering

For electrophoretic light scattering, samples were prepared by allowing proteins to adsorb to silica particles with a diameter of 3 μm. Protein solutions were added to nanoparticle suspensions while vigorously stirring (vortexing) to stop nanoparticles forming clusters. The surface charge of the particles were determined by electrophoretic light scattering using a Malvern Zetasizer Nano ZS fitted with a 633 nm laser. The zeta potential (ξ) of the particles was estimated from the electrophoretic mobility (u), according to the Helmholtz-Smoluchowski equation:

$$u = \epsilon \frac{\xi}{\eta}$$

where η is the viscosity, and ϵ is the dielectric constant. 0.5 mL of each bead solution was used in DTS1070 Folded Capillary Zeta Cells.

2.5. Interfacial Rheology

Interfacial rheology was carried out using a Discovery Hybrid Rheometer 3 from TA Instruments. The following protocol was used to characterise the interfaces shown in Supplementary Table S1. First, the denser of the two phases was added to the PTFE trough (19 mL) and the height of the liquid zeroed by measuring the normal force whilst lowering the Du Nouy ring until the 'pull in' force is observed. The ring is then lowered to position the first liquid-air interface at the ring equatorial plane, before the second phase, either oil or aqueous depending on the density of the oil used, is added (20 mL). For samples without any protein the interfacial modulus is then directly measured using an oscillatory frequency sweep, from 0.001 – 0.1 Hz with a displacement of 10^{-4} rad. The relaxation profile is also recorded using a peak strain of 1% at a rate of 1 %/s, the strain is then held for 120 s. Where a protein nanosheet was studied, the first step is a time sweep initially without any protein. The protein is then added after 30 min and the time sweep is left to run for 3 h and 12 h, for nanosheets generated on the fluorinated and mineral oil, respectively. These times correspond to the time it took for the interfacial shear moduli to plateau and hence for the nanosheets to fully form. After the time sweeps, the frequency sweep and stress relaxation tests are performed as before. Finally an amplitude sweep is performed from 10^{-6} – 10^{-1} rad at 0.1 Hz.

2.6. Interfacial AFM

Interfacial AFM was performed using an NT-MDT Ntegra Atomic Force Microscope with Bruker ORC 8 – 10 Contact AFM Tips with spring constants of ~0.05 N/m. The spring constant for each tip used was measured using the Sader method [13]. Beads were attached to the tips using the SEM (Quanta 3D FEG, FEI, EU/USA) with a custom built AFM (Attocube GmbH, Germany) integrated. The AFM tips were etched using the focused ion beam (FIB) to ensure a flat area was available for bead attachment. The tip was then coated with SEMGLU within the SEM before being brought into contact and bonding a single silicon bead. Once the bead was attached the glue was cured using FIB. The tips were plasma oxidised before each experiment. Before testing the interfaces the tips were calibrated by indenting a silicon wafer in order to be able to convert the deflection in nA into nm.

Each interface was indented on three separate 1 x 1 μm areas over which 100 indentations were performed. The frequency of each indentation was 1 Hz. The indentation depth was kept between 500 – 1000 nm depending on the sample. A minimum of three samples for each condition were tested.

In order to predict indentation traces based on our modified Young-Laplace model, a script that outputs the force–displacement profiles based on the surface potentials of the indenter and interface respectively, the surface tension and the Young's modulus of the nanosheet was applied. The Genetic Algorithm function in MATLAB was used to iterate these 4 variable until a best fit was achieved. The Genetic Algorithm is an automated function that varies inputs to minimise the fitness function. The Genetic Algorithm was used to minimise the following fitness function FitnessFunction = @(myInput) norm([f_exp(:), d_exp(:)] - myFunc(myInput)), where myFunc is the modelling script (which outputs x-y data for the force-displacement curves), f_exp and d_exp are experimental force-displacement data, respectively, and norm is a function which normalises the vector or array.

2.7. Development of the modified augmented Young – Laplace model

This model, based on the augmented Young – Laplace equation, assumes a pressure balance between surface tension, gravitational forces (typically neglected) and the internal drop pressure. The contribution of the internal drop pressure also becomes negligible if the drop is sufficiently large relative to the capillary length. With these assumptions, the augmented Young – Laplace can be expressed as [11]:

$$D'' + \frac{1}{t}D' - \left(2 - \frac{a\Pi(D)}{\gamma}\right)D_0 = 0 \qquad (1)$$

where D is the distance between the AFM probe and oil phase, as shown in Figure 1, a is the probe radius, γ is the surface tension, Π is the disjoining pressure and t the non-dimensional radius, such that $t = \frac{r}{\sqrt{D_0 a}}$. The forces between the colloid and the oil droplet are assimilated to those between two parallel plates, as per the Derjaguin approximation.

Characterising the interfacial surface tension using the augmented Young – Laplace equation treats the fluid interface as a zero thickness surface and describes the pressure balance using a non-linear partial differential equation. The disjoining pressure is the rate of change of the interaction energy over the plate separation, simplified by considering only the electrostatic and van der Waals forces [11, 14]. The hydrodynamic drainage is presently neglected [12]. Electrostatic double layer forces are modelled using the DLVO theory with the Debye – Hückel approximation [11]:

$$\Pi_{el} = \frac{\varepsilon\varepsilon_0 \mathrm{k}^2[2\psi_{1o}\psi_{2o}(e^{-kD} + e^{-3kD}) + (\psi_{1o}^2 + \psi_{2o}^2)e^{-2kD}]}{(1 - e^{-2kD})^2} \qquad (2)$$

where, ε is the relative permittivity, ε_0 is the permittivity of free space, k is the Debye length and ψ_{1o} and ψ_{2o} are the surface potentials of the indenter and oil respectively. The van der Waals forces are then given by [11]:

$$\Pi_{vdW} = \frac{A}{6\pi D^3} \qquad (3)$$

where A is the Hamaker constant, of the order of 10^{-20} J. Based on the solution to the augmented Young – Laplace (4th order Runge – Kutta numerical solution), the force – piezo movement relationship can then be extracted [11]. Briefly, this is done by solving Equation 4 – 8:

$$G = \frac{aD_0}{\gamma}\int_0^\infty t\Pi\big(D(t)\big)dt \qquad (4)$$

$$H = \frac{aD_0}{\gamma}\int_0^\infty tln(t)\Pi\big(D(t)\big)dt \qquad (5)$$

$$\mathrm{X}(D_0) = X_\infty + D_0 + H(D_0) + G(D_0)(1/2\ln(D_0) + B) \qquad (6)$$

$$\text{where, } B = C + ln\left(\frac{a^{1/2}}{2\lambda}\right) \qquad (7)$$

$$F_{interface}(D_0) = 2\pi\gamma G(D_0) \qquad (8)$$

where, C is Euler's constant, λ is the capillary length, X is the distance from the substrate to the lowest point of the colloidal probe and B is a constant dependent on the properties of the isolated interface. Here, G and H are the pressure differences across the interface within the deformation and externally, respectively. Using these calculations the force acting on the indenter probe, $F_{interface}$, can be plotted against the piezo crystal movement and compared to experimental data.

3. Results and Discussion

3.1. Comparison of shear and indentation moduli of liquid-liquid interfaces

To characterise the mechanical properties of nanosheets assembled at the surface of oil droplets, we proposed to extend a model describing the approach of a rigid probe deforming a liquid interface (Figure 1) [11, 12, 14, 15]. This model, based on the augmented Young – Laplace equation, assumes a pressure balance between surface tension, gravitational forces (typically neglected) and the internal drop pressure.

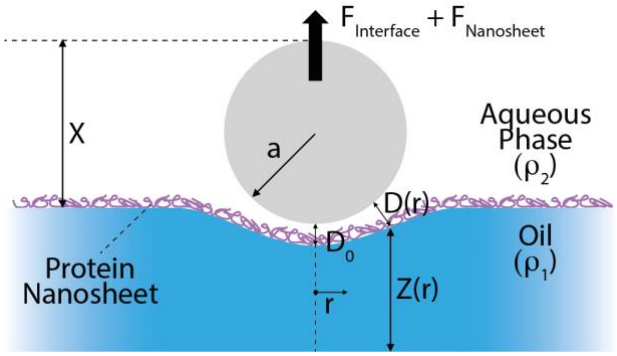

Figure 1. Schematic representation of the model of indentation of a hard sphere on a nanosheet assembled at a liquid-liquid interface. The model proposed is centrosymmetric. D_0 and $D(r)$ are the distance between the AFM probe and oil phase at the centre of the probe projected area and at a distance r from this centre. Z(r) is the height of the oil-water interface at a distance r from centre of the probe projected area. a is the probe radius, γ is the surface tension, ρ_1 and ρ_2 the densities of the oil and aqueous phase, respectively. X is the distance between the apex of the probe and the position of the undisturbed oil-water interface. $F_{Interface}$, is the force arising from the disjoining pressure on the

probe and $F_{nanosheet}$ is the force exerted on probe as a result of elastic deformation of the nanosheet. The sum of these two forces corresponds to F_{probe}

To confirm the validity of this model, we characterised the indentation profile of two oil-water interfaces, focusing on the fluorinated oil Novec 7500 and mineral oil, owing to their relevance as substrates for cell culture and protein nanosheet assembly [7, 16, 17]. In addition, we explored how the pro-surfactant pentafluorobenzoyl chloride (PFBC), which plays an important role in regulating the mechanical properties of protein nanosheets [7], altered the indentation profile of corresponding interfaces. The surface tension of these interfaces was characterised by tensiometry and the surface potential of the colloids used was determined via electrophoretic light scattering (Table 1). The results of this modelling and comparisons with experimental data are presented in Figure 2. The Hamaker constant, dielectric permittivity and Debye length used for modelling are gathered in Supplementary Table S2.

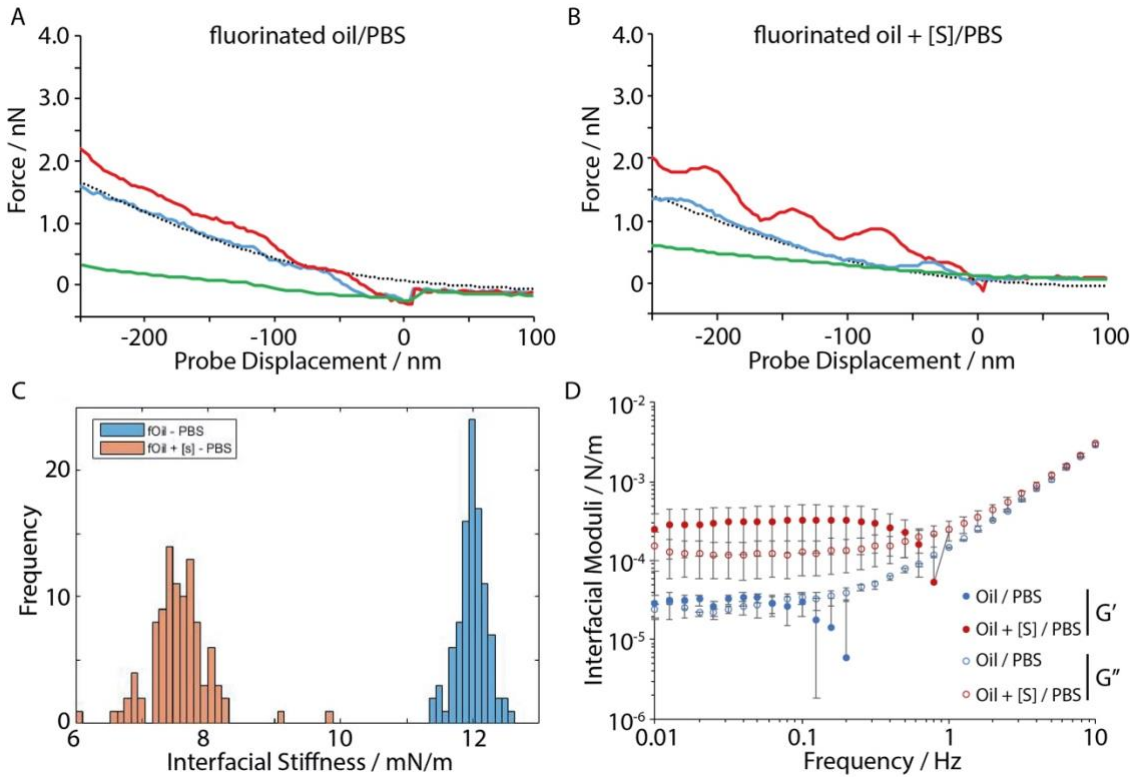

Figure 2. A-B) Comparison between representative experimental Force – Probe displacement traces and predictions based on the augmented Young – Laplace model for a fluorinated oil (Novec 7500) / PBS (A) and fluorinated oil (Novec 7500) supplemented with PFBC ([S] = 10 mg/mL; B) interface. Red, green and blue lines show representative curves for the upper and lower quartiles and average, respectively. The black dotted line represent the modelled data with parameters corresponding to Table 1. C) Histograms showing the spread in interfacial stiffness obtained over a 100 point scan by interfacial nanoindentation by AFM on fluorinated oil – PBS (blue) and fluorinated oil +[s] – PBS (red) interfaces. D) Interfacial rheology frequency sweeps of Novec 7500 – PBS interfaces without (blue) and with PFBC (at a concentration [S] of 0.01 mg/mL; red). Oscillating displacement of 10^{-4} rad. Error bars are standard deviations.

We observed an excellent agreement between predicted indentation profiles and average experimental traces (Figure 2B and Supplementary Figure S1), even at large indentation depths. A clear reduction in the stiffness of the oil-water interface was observed in the presence of the pro-surfactant PFBC

(Figure 2C). This is in good agreement with the modest decrease in surface tension observed in the presence of this molecule (Table 1), expected from its partial hydrolysis at the liquid-liquid interface. The surface potential of the colloid (ψ_{1o}) was approximated to the ζ-potential measured for this colloid. The predicted surface potential of the oil-water interfaces (ψ_{2o}) was found to be relatively small and negative (Table 1). Although this is in agreement with the neutral structure of the oils studied and the weak tensioactive properties of PFBC, these surface potentials are weaker than those measured for alkanes [18, 19, 20] and fluoroalkanes [21], perhaps due to the high ionic strength of the aqueous phase used in our study (PBS). The relatively low predicted ψ_{2o} may also result from a modest sensitivity of the model to this parameter. We also note some spread in the data with moderately polydisperse distribution of moduli observed whether on naked oil interfaces or in the presence of PFBC (Figure 2C and Supplementary Figure S1C). As liquid interfaces are expected to be relatively homogenous at the probe length scale, we propose that the observed heterogeneity is the result of slight variations in the approach angle, inherent of the quasi-hemispherical of the droplets characterised and the size of the scanned areas (1 by 1 μm), as well as slight variations in the contact angle of the pinned droplet characterised [22].

Table 1. Parameters used for modelling interfacial indentation data in Figure 2 and Figure S1 for interfaces fluorinated oil (fOil, Novec 7500) and mineral oil (mOil), with and without the pro-surfactant PFBC ([S] = 0.01 mg/mL).

Interface	Z-Potential		Surface Tension
	Ψ_{01} (mV)[a)]	Ψ_{02} (mV)[b)]	γ (mN/m)[c)]
fOil / PBS	-19.7	-5.0	44.5
fOil + [s] / PBS	-19.7	-5.0	37.0
mOil / PBS	-19.7	-4.5	25.0
mOil + [s] / PBS	-19.7	-4.5	16.0

[a] Determined via electrophoretic light scattering of the corresponding colloids. [b] Extracted from the model. [c] Liquid-liquid surface tension determined via tensiometry.

We next compared the macroscale interfacial rheology profile of liquid-liquid interfaces, using a Du Nouy ring fitted on a rheometer [9] with the results of our AFM indentation data. The interfacial shear moduli of the Novec 7500 and mineral oil interfaces with PBS were found to be $3.0\ 10^{-5} \pm 5.7\ 10^{-6}$ N/m and $1.2\ 10^{-3} \pm 4.38\ 10^{-4}$ N/m, respectively (Figures 2D and 3, Supplementary Figure S1D). The interfacial shear modulus of the fluorinated oil, in particular, is significantly lower than the indentation modulus of the corresponding interface. This is in agreement with the anisotropy of liquid-liquid interfaces, which are associated with surface tension and disjoining pressure contributing to shaping the deformation profile of the interface in the normal direction, whereas these parameters do not contribute to interfacial shear properties of naked fluid interfaces, associated with low viscosity and a fluid behaviour. Strikingly, whereas the stiffness of the oil-PBS interfaces decreased in the presence of pro-surfactants, the interfacial viscosity and shear moduli increased, due to the occurrence of intramolecular interactions at the corresponding interfaces. Indeed, the interfaces retained a clear viscous profile, with a marked frequency dependency and interfacial shear loss moduli spanning nearly two orders of magnitude (Figures 2D, Supplementary Figure S1D).

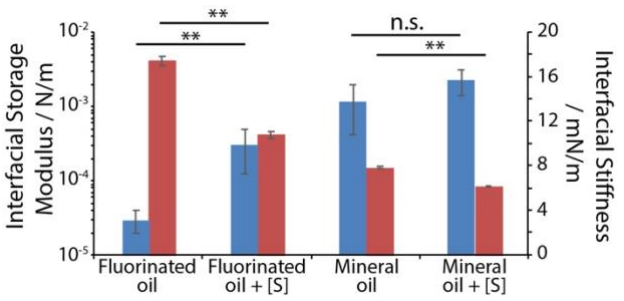

Figure 3. Summary of stiffness and interfacial rheology data obtained for fluorinated oil (Novec 7500) and mineral oil, with and without pro-surfactants (fluorinated oil, PFBC, [S] = 0.01 mg/mL; mineral oil, benzoyl chloride, [S] = 0.1 mg/mL). Blue, interfacial storage modulus; Red, interfacial stiffness. Errors are standard errors. n.s., not significant; **, $p<0.01$.

3.2. Mechanics of molecular films at liquid-liquid interfaces

We next characterised the AFM indentation profile of liquid-liquid interfaces at which protein nanosheets had been self-assembled (Figure 4 and Supplementary Figure S2). We found that the addition of BSA resulted in a decrease in the interfacial stiffness from 17.4 mN/m to 5.4 mN/m, while the addition of PLL did not significantly alter the mechanical profile of the interface (Figure 4A and C). This is in good agreement with the range of dilatational moduli reported for globular proteins self-assembling at liquid interfaces, such as casein and lysozyme, although without pro-surfactant [10, 23, 24]. In contrast, interfacial rheology indicated an increase in the storage moduli of interfaces at which protein nanosheets had been adsorbed, by 3-4 orders of magnitude (Figure 4B, 2D and Supplementary Figure S2B). Strikingly, interfaces at which BSA and PLL nanosheets were self-assembled displayed interfacial shear moduli of 0.6 ± 0.3 and 2.5 ± 0.2 N/m, respectively. Compared to pristine oil-PBS interfaces, BSA nanosheets displayed 10^4 fold increase in interfacial shear storage modulus and PLL nanosheets a 10^5 fold increase. Therefore, the anisotropy in interfacial mechanics (defined as the ratio of the interfacial shear storage modulus by the interfacial stiffness) was found to switch from $1.7\ 10^{-3}$ for naked oil-PBS interfaces to 83 and 152 in the presence of BSA and PLL nanosheets, respectively. This switch therefore spans several orders of magnitude and the ultimate mechanical anisotropy is the highest reported in the literature, to the best of our knowledge. Indeed, some of the most

anisotropic mechanical systems, such as bone, wood and processed self-assembled block copolymers display mechanical anisotropies in the range of 1.5 to 6.5 [25, 26, 27, 28, 29]. We propose that this unique phenomenon originates from the unique combination of physico-chemical properties regulating interfacial mechanics. Indeed, whereas transvers indentation of interfaces is regulated by surface tension and the disjoining pressure, as well as the elastic properties of molecular films assembled at corresponding interfaces, in-plane interfacial shear properties are solely regulated by the mechanics of interfacial molecular films.

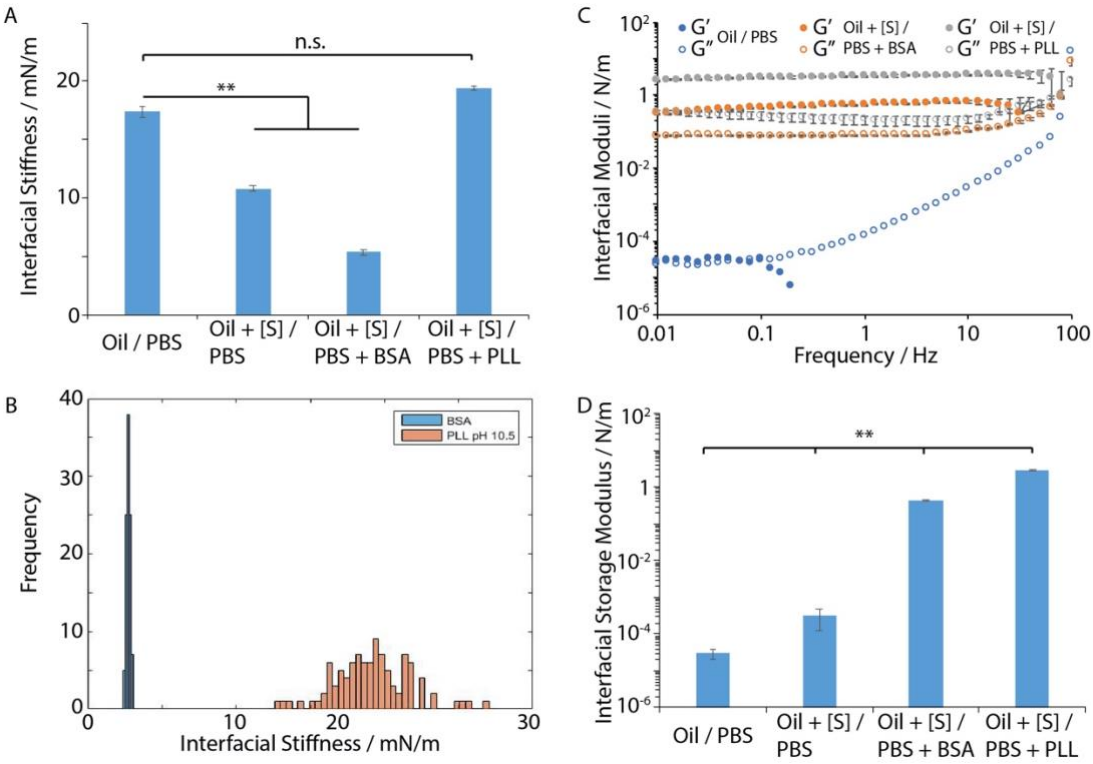

Figure 4. AFM indentation and interfacial rheology of protein nanosheets assembled at liquid-liquid interfaces. A) Average interfacial stiffness of fluorinated oil interfaces (Novec 7500) with and without pro-surfactant PFBC (0.01 mg/mL) and with BSA (1 mg/mL) and PLL (100 μg/mL, deposition at pH 10.5) nanosheets. B) Corresponding distribution of interfacial stiffness obtained for BSA and PLL nanosheets. C) Interfacial storage and loss moduli of fluorinated oil interfaces (Novec 7500) prior and after self-assembly of protein nanosheets in the presence of pro-surfactant PFBC (0.01 mg/mL). Nanosheets: BSA (1 mg/mL) and PLL (100 μg/mL, deposition at pH 10.5). D) Interfacial storage moduli of corresponding interfaces, at a frequency of 0.1 Hz (strain of 10^{-4} rad). Frequency sweeps with strains of 10^{-4} rad. Errors are standard errors. n.s., not significant; **, $p<0.01$.

3.3. Disentanglement of Parameters Controlling the AFM Indentation Profile of Molecular Films at Liquid-Liquid Interfaces

In order to model the AFM indentation data obtained and disentangle the different contributions to corresponding indentation profiles, we adapted the Young-Laplace model with a model of a molecular film or shell, representing the protein nanosheet [30]. This model assumes a thin rigid shell, as shown in Figure 1, subjected to a linear elastic shear. In the case of supported membranes (as for pinned droplets), at low indentation, the bending deformation of the membrane can be neglected and shear mechanics alone considered. The corresponding governing equation describing the force-displacement profile is [30]:

$$v = \frac{(1+\upsilon)F_{nanosheet}{a_{drop}}^2}{E}\left[\sin\varphi\ln(1+\cos\varphi) - \frac{\sin\varphi}{1+\cos\varphi}\right] \quad (9)$$

where, v is the strain applied on the film, φ is the angle of the shell at the meridian plane, E is the Young's modulus of the film, υ is the Poisson ratio, a_{drop} is the radius of the droplet and $F_{\text{nanosheet}}$ is the applied force. The total force acting on the AFM probe, F_{probe}, is the sum of forces corresponding to the shell elasticity, $F_{nanosheet}$, and the interfacial mechanical force corresponding to the disjoining pressure:

$$F_{probe} = F_{interface} + F_{nanosheet} \quad (10)$$

We numerically solved this equation using a genetic algorithm to iterate 4 variables (the surface potentials of the indenter and interface, the surface tension and the Young's modulus of the film). The quality of the fit was assessed using the standard error of the estimate, quantifying the average distance of the predicted displacement to that measured.

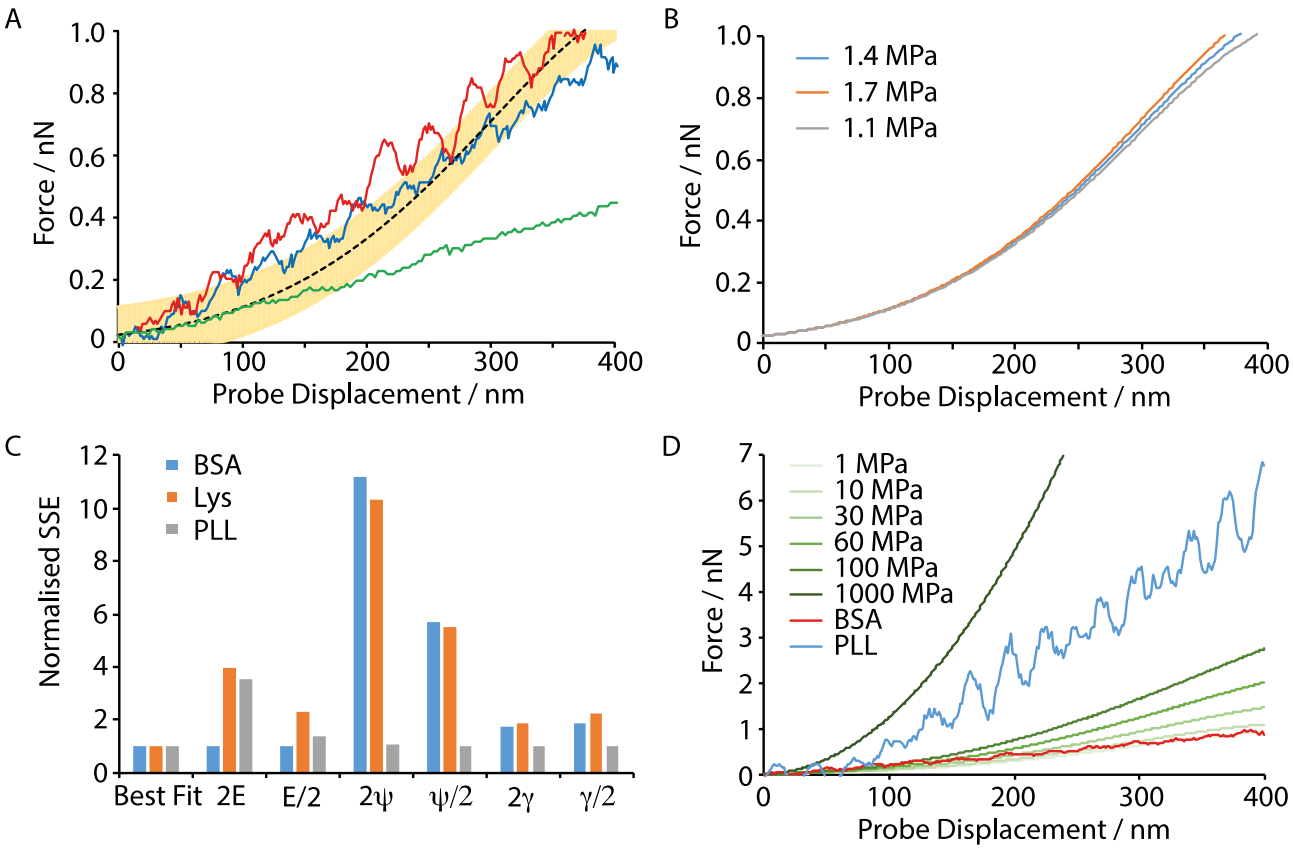

Figure 5. Theoretical force-indentation profile for BSA nanosheets adsorbed at Novec 7500 – PBS interfaces (in the presence of PFBC at 0.01 mg/mL). A) Compared to representative experimental data (mean, upper and lower quartiles; blue, red and green lines respectively). Parameters used for the best fit are shown in tables 1 and 3. Yellow error bars represent the SEE of the best fit to representative mean data. B) Sensitivity of the model to variation in modulus. C) Standard error of the estimate (SEE) comparison calculated when altering the surface potential, surface tension and Young's modulus (factor of 2), normalised against the SEE of the best fit, for interfaces presenting BSA, PLL and lysozyme nanosheets. D) Predictions of the mechanical response of a BSA nanosheet reinforced interface (surface potentials and surface tension corresponding to fit data), varying the nanosheet modulus from 1 – 1000 MPa, compared to the experimental data obtained for the average PLL and BSA data.

Results of the combined Young-Laplace model indicate an excellent fit with experimental data (Figure 5A and Supplementary Figure S3). Parameters used to obtain the lines of best fit are gathered in Table 2 and are in good agreement with parameters experimentally evaluated. Deviations from these parameters, especially the surface potential ψ_{2o} measured are likely to arise from the use of silica colloids coated with the corresponding proteins, instead of the protein-functionalised oil interfaces. Hence our revised model is able to account for the mechanics of molecular films assembled at liquid-liquid interfaces and extract quantitative mechanical data characterising protein nanosheets. Note that in the case of PLL nanosheets, we input positive surface potentials, corresponding to colloids at the surface of which PLL had been adsorbed, in agreement with the lack of adhesion observed in retraction traces and the predicted potential of the corresponding interfaces. It is also worth pointing out that the notion of surface tension in these systems, with protein nanosheets adsorbed at interfaces, is not fully appropriate, as the naked liquid-liquid interface has been replaced with a film, with limited further dynamic exchange with surrounding media.

Table 2. Parameters used for modelling interfacial indentation data in Figure 5 and Supplementary Figure S3-4, for protein nanosheets assembled at fluorinated oil (fOil, Novec 7500) and mineral oil (mOil) interfaces, in the presence of pro-surfactant (PFBC, [S] = 0.01 mg/mL, for BSA and PLL; benzoyl chloride, [S] = 0.1 mg/mL, for lysozyme, Lys).

	Ψ_{01} (mV)		Ψ_{02} (mV)		γ (mN/m)		E (MPa)	
	Exp[a)]	**Fit**	**Exp[b)]**	**Fit**	**Exp[c)]**	**Fit**	**Exp[d)]**	**Fit**
BSA	-20	-13	-21	-5	23	15	3.5	1.4
PLL	12	5	12	5	27	30	235	235
Lys	-20	-14	-7	-6	14	11	65.0	56.0

[a)]Determined via electrophoretic light scattering of the corresponding colloids. Note that for PLL nanosheets, the colloid was coated with PLL. [b)]Determined via electrophoretic light scattering of the corresponding colloids after protein adsorption. [c)]From liquid-liquid surface tension determined via tensiometry. [d)] Extracted from interfacial rheology data (considering the thickness of 14-19 nm for these nanosheets [7]).

In order to quantify the error associated with the parameters fitted in our model, we determined the standard error of the estimate (SEE) for the fits of the different conditions modelled. We then systematically varied each parameter independently by a factor of 2 and quantified the associated SEE. This allowed us to determine the normalised SEE, with respect to that of the best fit condition (Figure 5C). From this analysis, it is clear that the indentation profile of BSA nanosheets is particularly sensitive to changes in surface potential and surface tension, whilst variation in modulus have a minimal impact on the profiles. This is also apparent from the plot of predicted profiles from our modified model when varying each parameter independently (Figure 5B and Supplementary Figure S3). In contrast, the indentation profiles predicted for PLL nanosheets was more sensitive to the modulus of the nanosheets than to variation in surface potentials and surface tension (Supplementary Figure S4). Predictions for lysozyme nanosheets displayed intermediate levels of sensitivity to these different parameters, as clearly retaining some sensitivity to the modulus of the

film, but also displaying high sensitivities to surface potentials. In order to demonstrate more clearly the sensitivity of the indentation profile to the mechanical properties of the nanosheets self-assembled at corresponding liquid-liquid interfaces, we predicted the force-indentation traces for BSA nanosheets with moduli ranging from 1 MPa to 1000 MPa (Figure 5D). From this data, it is clear that indentation profiles are very sensitive to moduli above 100 MPa and that the disjoining pressure is dominating below this value. Therefore only the mechanical behaviour of relatively stiff molecular films assembled at liquid-liquid interfaces can be quantitatively characterised via AFM indentation.

3.4. Force probe microscopy to image nanoscale heterogeneity

Full and accurate quantification of protein nanosheet mechanics using AFM indentation therefore requires characterisation of associated surface potentials and tension. In this context, interfacial rheology appears more accurate, without requiring additional interfacial characterisation. However, AFM indentation, in particular coupled to fluorescence microscopy, enables to image mechanical heterogeneity in samples, an aspect ignored in interfacial rheology. To demonstrate this aspect, we correlated AFM indentation mapping and corresponding fluorescence microscopy images. Tagged PLL nanosheets were found to form domains spanning several tens of μm (Figure 6). We carried out 1 x 1 μm AFM indentation scans of these domains, aiming for the central area of a domain and its periphery. Although a relatively broad distribution of interfacial stiffnesses was observed in both areas, a clear softening was observed at the periphery of the domain, suggesting an unconfined boundary resulting in more pronounced displacements. We note that the relative spread of data may highlight a combination of mechanical heterogeneity (although nanosheets appear relatively homogenous within one domain by fluorescence microscopy) and change in the surface chemistry of the colloidal probe. Indeed, we observed some level of ageing of the tip as evidenced by a drift in the interfacial stiffness as a function of indentation number (Supplementary Figure S5).

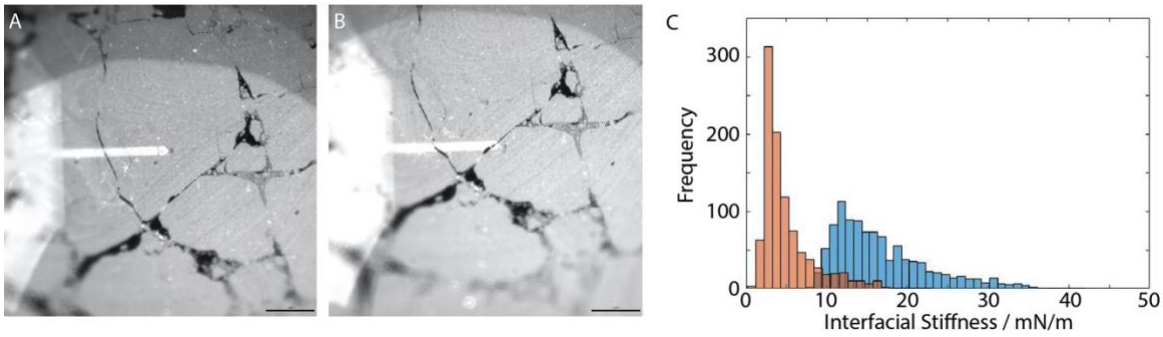

Figure 6. A-B) Epifluorescence images of tagged PLL nanosheets and the position of the AFM tip for scans in the centre (A) and at the edge (B) of domains. C) Histograms of distribution of interfacial stiffnesses obtained from AFM indentation scans at the centre (blue) and edge (red) of the domain. Scale bar (black line in bottom right corner), 80 μm. The white bar corresponds to the reflection of the cantilever.

4. Conclusion

In summary, comparison of AFM indentation and interfacial rheology clearly highlighted the extreme mechanical anisotropy of liquid interfaces reinforced with self-assembled molecular films, with anisotropy factors as high as 152, orders of magnitude higher than those observed for more conventional anisotropic materials. In addition, our work quantifies the remarkable switch in mechanical anisotropy that occurs upon the formation of a nanofilm at liquid interfaces. Such unique behaviour is proposed to arise from the vastly different origins of transverse (dominated by surface tension) and in plane interfacial shear mechanics (dominated by nanosheet mechanics). In turn, this anisotropy is proposed to have specific applications, for example for the design of emulsions enabling cell adhesion and cell expansion in 3D bioreactors. In this context, the high interfacial shear moduli that can be achieved with protein nanosheets, despite the modest change in transverse interfacial stiffness, enables resistance against cell-mediated contractile forces and sustains cell spreading. Although a detailed understanding of how the nanostructure of protein nanosheets correlates with

their mechanics and how this regulates cell adhesion and expansion is still required, the design of protein nanosheet-reinforced liquid-liquid interfaces will enable the development of new biotechnological platforms based on emulsions. The inherent anisotropy of these interfaces may also form the basis of novel strategies for the microstructuring of liquid and liquid crystalline droplets [6, 8].

The modified Young-Laplace model developed clearly demonstrates how quantitative information can be extracted from AFM indentation data at liquid-liquid interfaces stabilised by protein nanosheets. However, our quantitative analysis highlights the restricted parameter range in which this model can operate. This has obvious implications for the characterisation of molecular films, such as the nanosheets studied, but also for the characterisation of other soft interfaces, such as liquid-liquid interfaces stabilised by nanomaterials, as well as the characterisation of cell membrane mechanics via AFM indentation. Our data suggest that such characterisation requires the quantification of associated disjoining pressures (although surface tension is not defined in these systems). Macroscale interfacial rheology is of limited applicability in such cases. Hence this works clearly calls for the development of nano- to micro-scale rheological probes able to gain truly quantitative interfacial rheological data, at relevant mechanical scales, characterising soft interfaces.

Supporting Information

Supporting Information is available from Elsevier or from the corresponding author.

Acknowledgements

Funding for this work from the Engineering and Physical Sciences Research Council (EP/L505602/1) and the European Research Council (ProLiCell, 772462) is gratefully acknowledged. We thank Dr Russell Bailey for technical support with AFM indentation.

CRediT authorship contribution statement

William Megone: Conceptualization, Investigation, Methodology, Software, Writing - original draft. **Dexu Kong:** Investigation. **Lihui Peng:** Investigation. **Julien Gautrot:** Conceptualization, Funding acquisition, Supervision, Writing - review & editing.

References

[1] E. Parra, J. Pérez-Gil, Composition, structure and mechanical properties define performance of pulmonary surfactant membranes and films, Chem. Phys. Lipids 185 (2015) 153-175.
[2] I. Cooper, S.J. Vance, B.O. Smith, M.W. Kennedy, Frog foams and natural protein surfactants, Colloid Surf. A 534 (2017) 120-129.
[3] L. Hobley, A. Ostrowski, F.V. Rao, K.M. Bromley, M. Porter, A.R. Prescott, C.E. MacPhee, D.M.F. van Aalten, N.R. Stanley-Wall, BsIA is a self-assembling bacterial hydrophobin that coats the Bacillus subtllis biofilm, Proc. Natl. Acad. Sci. 110 (2013) 13600-13605.
[4] G.B. Brandani, M. Schor, R. Morris, N. Stanley-Wall, C.E. MacPhee, D. Marenduzzo, U. Zachariae, The Bacterial Hydrophobin BslA is a Switchable Ellipsoidal Janus Nanocolloid, Langmuir 31 (2015) 11558-11563.
[5] J. Forth, X. Liu, J. Hasnain, A. Toor, K. Miszta, S. Shi, P.L. Geissler, T. Emrick, B.A. Helms, T.P. Russell, Reconfigurable Printed Liquids, Adv. Mater. 30 (2018) 1707603.
[6] N. Denkov, S. Tcholakova, I. Lesov, D. Cholakova, S.K. Smoukov, Self-shaping of oil droplets via the formation of intermediate rotator phases upon cooling, Nature 528 (2015) 392-395.
[7] D. Kong, W. Megone, K.D.Q. Nguyen, S. di Cio, M. Ramstedt, J.E. Gautrot, Protein nanosheet mechanics controls cell adhesion and expansion on low-viscosity liquids, Nano Lett. 18(3) (2018) 1946-1951.
[8] W.-S. Wei, Y. Xia, S. Ettinger, S. Yang, A.G. Yodh, Molecular heterogeneity drives reconfigurable nematic liquid crystal drops, Nature 576 (2019) 433-436.
[9] G.G. Fuller, J. Vermant, Complex fluid-fluid interfaces: rheology and structure, Annu. Rev. Chem. Biomol. Eng. 3 (2012) 519-543.
[10] M.A. Bos, T. van Vliet, Interfacial rheological properties of adsorbed protein layers and surfactants: a review, Adv. Colloid Interf. Sci. 91 (2001) 437-471.
[11] D.Y.C. Chan, R.R. Dagastine, L.R. White, Forces between a rigid probe particle and a liquid interface: I. the repulsive case, J. Colloid Interf. Sci. 236 (2001) 141-154.
[12] R.R. Dagastine, L.R. White, Forces between a Rigid Probe Particle and a Liquid Interface: II. The General Case, J. Colloid Interf. Sci. 247(2) (2002) 310-320.
[13] J.E. Sader, J.W.M. Chon, P. Mulvaney, Calibration of rectangular atomic force microscope cantilevers, Review of Scientific Instruments 70(10) (1999) 3967-3969.
[14] D.E. Aston, J.C. Berg, Quantitative Analysis of Fluid Interface–Atomic Force Microscopy, J. Colloid Interf. Sci. 235(1) (2001) 162-169.
[15] B.A. Snyder, D.E. Aston, J.C. Berg, Particle-drop interfactions examined with an atomic force microscope, Langmuir 13(3) (1997) 590-593.
[16] D. Kong, K.D.Q. Nguyen, W. Megone, L. Peng, J.E. Gautrot, The culture of HaCaT cells on liquid substrates is mediated by a mechanically strong liquid-liquid interface, Faraday Discuss. 204 (2017) 367-381.
[17] D. Kong, L. Peng, S. di Cio, P. Novak, J.E. Gautrot, Stem cell expansion and fate decision on liquid substrates are regulated by self-assembled nanosheets, ACS Nano 12(9) (2018) 9206-9213.
[18] A. Wiacek, E. Chibowski, Zeta potential, effective diameter and multimodal size distribution in oil:water emulsion, Colloid Surf. A 159 (1999) 253-261.
[19] R. Dagastine, T.T. Chau, D.Y.C. Chan, S.G. W, F. Grieser, Interaction forces between oil–water particle interfaces—Non-DLVO forces, Faraday Discuss. 129 (2005) 111-124.
[20] F. Yang, W. Wu, S. Chen, W. Gan, The ionic strength dependent zeta potential at the surface of hexadecane droplets in water and the corresponding interfacial adsorption of surfactants, Soft Matter 13 (2017) 638-646.
[21] D.S. Li, S. Schneewind, M. Bruce, Z. Khaing, M. O'Donnell, L. Pozzo, Spontaneous Nucleation of Stable Perfluorocarbon Emulsions for Ultrasound Contrast Agents, Nano Lett. 19 (2019) 173-181.
[22] D.C. Bardos, Contact angle dependence of solid probe–liquid drop forces in AFM measurements, Surf. Sci. 517 (2002) 157-176.

[23] E.M. Freer, K.S. Yim, G.G. Fuller, C.J. Radke, Interfacial rheology of globular and flexible proteins at the hexadecane/water interface: comparison of shear and dilatation deformation, J. Phys. Chem. B 108 (2004) 3835-3844.
[24] E.M. Freer, K.S. Yim, G.G. Fuller, C.J. Radke, Shear and dilatational relaxation mechanisms of globular and flexible proteins at the hexadecane/water interface, Langmuir 20 (2004) 10159-10167.
[25] J. Seto, H.S. Gupta, P. Zaslansky, H.D. Wagner, P. Fratzl, Tough Lessons From Bone: Extreme Mechanical Anisotropy at the Mesoscale, Adv. Funct. Mater. 18 (2008) 1905-1911.
[26] J. Song, C. Chen, Z. Yang, Y. Kuang, T. Li, Y. Li, H. Huang, I. Kierzewski, B. Liu, S. He, T. Gao, S.U. Yuruker, A. Gong, B. Yang, L. Hu, Highly Compressible, Anisotropic Aerogel with Aligned Cellulose Nanofibers, ACS Nano 12 (2018) 140-147.
[27] J.L. Katz, P. Spencer, Y. Wang, A. Misra, O. Marangos, L. Friis, On the anisotropic elastic properties of woods, J. Mater. Sci. 43 (2008) 139-145.
[28] J. Stasiak, A.M. Squires, V. Castelletto, I.W. Hamley, G.D. Moggridge, Effect of Stretching on the Structure of Cylinder- and Sphere-Forming Styrene-Isoprene-Styrene Block Copolymers, Macromolecules 42 (2009) 5256-5265.
[29] Y. Cang, Z. Wang, C. Bishop, L. Yu, M.D. Ediger, G. Fytas, Extreme Elasticity Anisotropy in Molecular Glasses, Adv. Funct. Mater. 30 (2020) 2001481.
[30] P. Marti, Theory of Structures : Fundamentals, Framed Structures, Plates and Shells, Wilhelm Ernst & Sohn Verlag fur Architektur und Technische, Berlin, 2013.